drones

Article

Experimentally Determining Optimal Conditions for Mapping Forage Fish with RPAS

Nicola R. Houtman [1,*], Jennifer Yakimishyn [2], Mike Collyer [2], Jennifer Sutherst [3], Cliff L. K. Robinson [4] and Maycira Costa [1]

[1] Department of Geography, University of Victoria, 3800 Finnerty Road, Victoria, BC V8P 5C2, Canada
[2] Pacific Rim National Park Reserve, Parks Canada Agency, P.O. Box 280, Ucluelet, BC V0R 3A0, Canada
[3] Comox Valley Project Watershed Society, 2356 Rosewall Crescent, Courtenay, BC V9N 8R9, Canada
[4] Pacific Biological Station, Department of Fisheries and Oceans Canada, 3190 Hammond Bay Road, Nanaimo, BC V9T 6NT, Canada
* Correspondence: nicolahoutman@gmail.com

Abstract: RPAS (Remotely piloted aircraft systems, i.e., drones) present an efficient method for mapping schooling coastal forage fish species that have limited distribution and abundance data. However, RPAS imagery acquisition in marine environments is highly dependent on suitable environmental conditions. Additionally, the size, color and depth of forage fish schools will impact their detectability in RPAS imagery. In this study, we identified optimal and suboptimal coastal environmental conditions through a controlled experiment using a model fish school containing four forage fish-like fishing lures. The school was placed at 0.5 m, 1.0 m, 1.5 m, and 2.0 m depths in a wide range of coastal conditions and then we captured RPAS video imagery. The results from a cluster analysis, principal components, and correlation analysis of RPAS data found that the optimal conditions consisted of moderate sun altitudes (20–40°), glassy seas, low winds (<5 km/h), clear skies (<10% cloud cover), and low turbidity. The environmental conditions identified in this study will provide researchers using RPAS with the best criteria for detecting coastal forage fish schools.

Keywords: RPAS; forage fish; marine aerial survey; environmental conditions; UAS; UAV

Citation: Houtman, N.R.; Yakimishyn, J.; Collyer, M.; Sutherst, J.; Robinson, C.L.K.; Costa, M. Experimentally Determining Optimal Conditions for Mapping Forage Fish with RPAS. *Drones* **2022**, *6*, 426. https://doi.org/10.3390/drones6120426

Academic Editors: Barbara Bollard and Margarita Mulero-Pázmány

Received: 18 October 2022
Accepted: 12 December 2022
Published: 17 December 2022

1. Introduction

Remotely piloted aerial vehicles (RPAS) are a valuable tool for conservation since they became commercially available around 2010 [1,2]. RPAS offer a non-invasive, flexible, cost-effective method to quickly survey large areas (~8 min for 1 km^2 coverage) and collect high resolution, spatially explicit imagery that can be used to map or monitor the distribution of marine organisms such as turtles and marine mammals [1–4]. Smaller, more cryptic, and under sampled forage fish species that school near the sea surface could also greatly benefit from RPAS surveys [1,5].

Forage fish play a critical role in marine ecosystems by providing a trophic link between plankton and piscivorous fish, mammals, and marine birds [6]. They are crucial to maintaining healthy ecosystems, contribute directly and indirectly to the economic value of global fisheries, and support the conservation and recovery of many coastal marine species at risk [7,8]. Currently in British Columbia, Canada, Pacific Herring (*Clupea pallasii*), Pacific Sand Lance (*Ammodytes personatus*; "Sand Lance") and, to a lesser extent, Northern Anchovy (*Engraulis mordax*) are thought to be the most ecologically important coastal forage fish [9–11]. These species are prey to many ecologically and economically valuable predators such as the Chinook salmon (*Oncorhynchus tshawytscha*) and the threatened marbled murrelet (*Brachyramphus marmoratus*) [11–15]. Despite their importance, information about the abundance and distribution of many of BC's forage fish is limited [11,16,17].

A variety of methods can be used to quantify the abundance and distribution forage fish, but many cannot access shallow areas, are size selective or destructive, and are subject

to fish avoidance [1,18]. By comparison, RPAS offer a non-destructive, cost and time effective method to survey tens of square kilometers of shallow nearshore habitats that are important to small surface schooling forage fish species such as Sand Lance and Pacific Herring [19,20].

RPAS surveys capture visible spectra (blue, green, red) imagery of the ocean, targeting subsurface features, and are typically limited by environmental conditions (e.g., wind, waves, sun angle, cloud cover, turbidity) and target characteristics (e.g., target depth, color, size)]. Environmental conditions such as wind, waves, sun altitude, clouds, and turbidity can affect the appearance of the sea surface in the imagery and the light penetration into the water column [4,21,22]. Furthermore, RPAS imagery is only able to capture under-water targets in the visible wavelengths due to water light attenuation properties in other parts of the spectra [23–25]. In order to reduce availability errors, surveys must generally be conducted under calm, clear conditions, and occur when targets are in the visible portion of the water column to ensure that targets within the sampled area are available to be seen [23,25]. Finally, larger targets with contrasting colors to the background are more readily detected in RPAS imagery [23,24,26]. Given these considerations, target-specific standardized protocols are required for repeatable and comparable surveys [5,19,21,23,26,27]. Some research has described general protocols for mapping submerged targets [21] and others have looked at protocols for specific taxa or benthic habitat types [5,22,28]. However, no RPAS protocols have been developed specifically for forage fish surveys including evaluating for the most optimal environmental conditions [1,5].

The main objective of this study was to develop a data acquisition protocol defining optimal environmental conditions for detecting forage fish in coastal waters using RPAS imagery. Environmental conditions for detecting forage fish were evaluated through infield experiments using forage fish-like fishing lures and considering the influence of sun altitude, turbidity (secchi depth as a proxy), cloud cover, wind speed, and wave height. Generally, our findings showed that calm conditions with clear skies, moderate sun angles, and low turbidity to be optimal, similar to others working with different taxa, including eelgrass, sharks, and marine mammals [4,5,21–23,28–33]. Defining these optimal conditions will help make RPAS surveys the basis of a practical, efficient, non-destructive, fishery independent technique for quantifying forage fish distribution and abundance [5]. Furthermore, this research can inform RPAS survey design of other surface-schooling forage fish in other locations globally that have similar morphologies to the lures used in this experiment.

2. Materials and Methods

2.1. Study Area

The study area comprised of two coastal regions of varying oceanographic and environmental conditions on southern Vancouver Island, British Columbia (Figure 1). The majority of the environmental samples (samples defined in Section 2.2) were recorded at Nettle Island within the Broken Group Islands (BGI) in Barkley Sound which is part of the Pacific Rim National Park Reserve (PRNPR) on the southwest coast of Vancouver Island. The BGI supports high fish diversity including Shiner Perch (*Cymatogaster aggregata*), Pacific Sand Lance, and Pacific Herring among other species [34–36]. The BGI opens to the Pacific Ocean on the windward side of Vancouver Island which drives the wet and cool climate, causing overcast and fog conditions in the spring and summer [37]. Data acquisition in the BGI occurred during mornings in May and early June to target the calmest conditions and to avoid phytoplankton blooms and foggy conditions that occur in July and August (Personal communication, Jennifer Yakimishyn, June 2020). The RPAS surveys in the BGI captured most environmental conditions of interest, except the combination of clear skies and high wind.

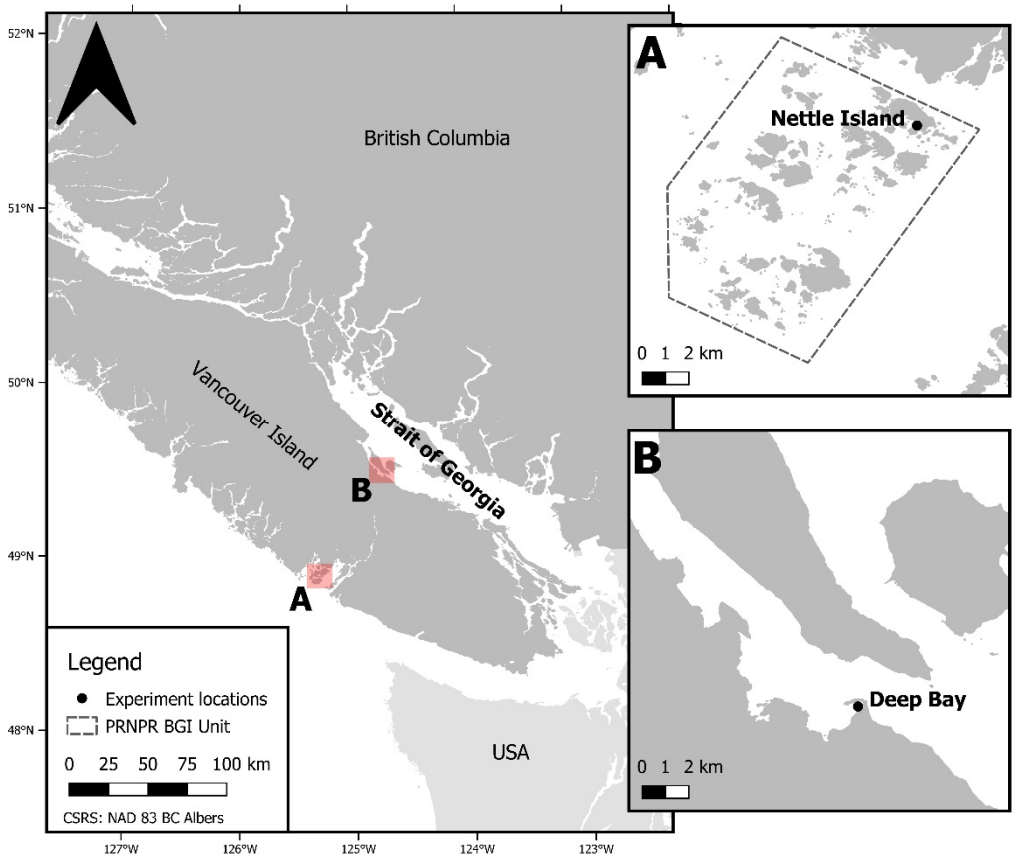

Figure 1. The study area map showing the location of the experiment locations at Nettle Island in the BGI (map panel **A**) on the west coast of Vancouver Island and at Deep Bay in Baynes Sound (map panel **B**) on the east coast of VI, in the Strait of Georgia.

The second study site, Baynes Sound, was located on the eastern coast of Vancouver Island in the Strait of Georgia (Figure 1). Baynes Sound has a large range of nearshore habitats that support a high biomass of numerous forage fish species, including Pacific Herring, Sand Lance and Northern Anchovy, among others [38–40]. Baynes Sound lies on the leeward side of Vancouver Island in a rain shadow and has warmer and drier conditions than the BGI [37]. Three samples were recorded at Deep Bay in Baynes Sound to capture conditions that had not been encountered in the BGI. A single field day (19 August 2021) was sufficient to complete the data acquisition in Baynes Sound.

2.2. Data Collection

The data collection included capturing RPAS imagery at a set altitude of 15 m of an experimental model fish school located at four fixed depths below the sea surface and recording the environmental variables that occurred during each experimental imagery sample. As such, each sample included imagery of the model fish school at four different depths and a recorded value of each environmental variable (including wind speed, wave height, sun altitude, cloud cover, and secchi depth) that occurred during the imagery acquisition. The model forage fish school was comprised of four types of fishing lures (10 of each type) that mimicked forage fish colors and sizes (Figure 2). The lures mimicked previously observed local forage fish (seen in test RPAS forage fish surveys completed in 2020) and contained the foundational counter-shading color scheme of most near-surface schooling pelagic fish [41,42]. The two main categories of forge fish detections seen in the test forage fish RPAS surveys: (1) dark fish visible over light bottoms and (2) "fish flashes" seen as a brief flash of bright light in videos as fish turned on their side reflecting light into the sensor. Dark fish over light bottom detections were likely Shiner Perch, while fish

flash detections were mostly Herring and Sand Lance. The dark fish over light bottoms are represented by a dark lure (lure A, Figure 2) while the fish flashes are represented by silver lures (lures B, C, D, Figure 2). Two quadrats of 0.75 m^2 each had 20 randomly placed lures. Quadrat 1 had ten 10 mm long black lures (lure A in Figure 2) and ten 11 mm long metal lures (lure B in Figure 2) representing the dark Shiner Perch and Sand Lance fish flashes, respectively. Quadrat 2 had the same silver lure type in 9 cm and 5 cm long (lures C and D in Figure 2; ten of both lure types), representing fish flashes from juvenile and adult Herring, respectively.

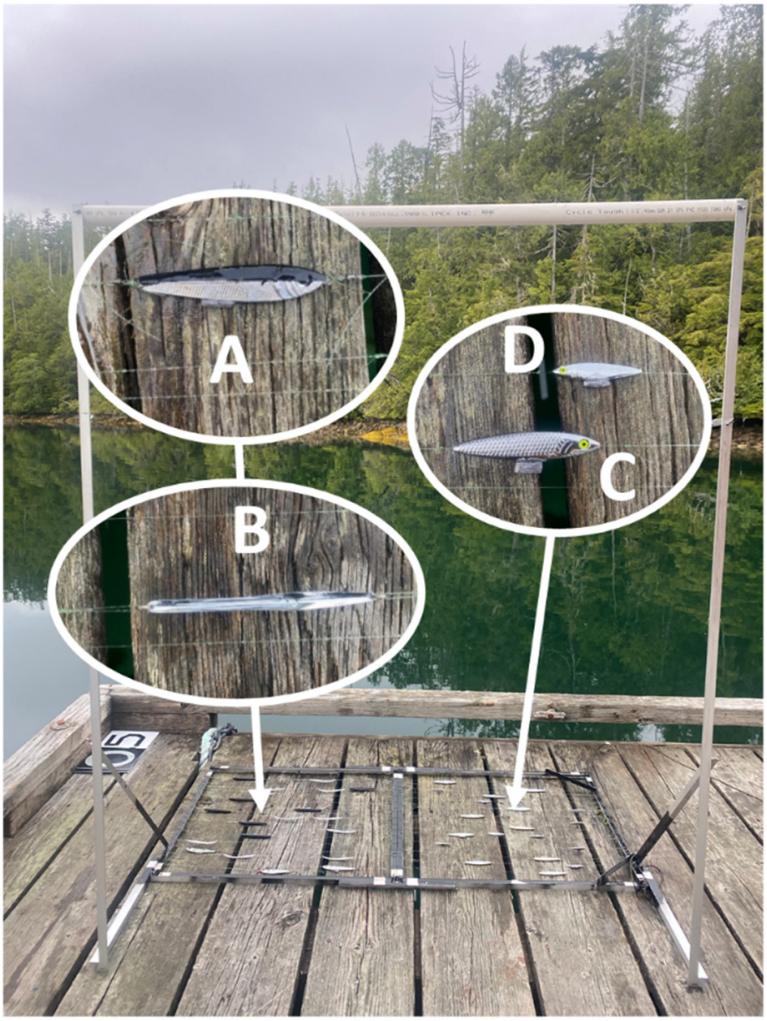

Figure 2. The model fish school with two quadrats and ten of four different fish lures that represent dark, counter shaded fish (lure A), Sand Lance fish flashes (lure B), and adult and juvenile herring fish flashes (lures C and D). The upright posts and cross bar allow researchers to lower the quadrats up to 2 m depth. The quadrat frames were painted black with silver squares at the vertices for easy visual locating of the model fish school in the RPAS imagery. Note the small lead weights attached to the bottom of lures A, C, and D to keep them oriented in an upright position in all imagery samples (not needed for lure B).

The model fish school was placed at 0.5 m, 1.0 m, 1.5 m, and 2.0 m depths, which represents the approximate depths of forage fish schools observed from small boats in the test RPAS surveys. With the model fish school positioned at the specified depths, triplicate RPAS imagery (5 s of 4 k video for each model fish school depth) were acquired at 15 m elevation above the sea surface. The videos recorded at each depth were taken approximately 30 s apart as each depth was recorded first (first triplicate) before recording the second and then the third triplicate. The environmental conditions were monitored

to ensure no change between triplicate samples. Logistics allowed a total of 127 triplicate samples, 124 of which were recorded a Parks Canada dock at Nettle Island in the BGI with a Mavic 2 Professional (M2P) RPAS and three samples were recorded at a marina dock in Deep Bay with a Phantom 4 (P4). This sample size included samples of all the conditions thought to be important based on test forage fish RPAS surveys and recommendations in the literature. All samples were comparable as both RPAS have similar sensors (Table 1) and they were recorded at nadir angles at a flight altitude of 15 m above the sea surface. In addition, the sea floor (10–20 m depth) was not visible at either dock, which kept a standardized background of a deep water column for all samples.

Table 1. The specifics on the RPAS models used.

	M2P		**P4**
Study area used	BGI		SOG
Ground sampling distance at 15 m height	0.5 cm (video)		0.67 cm (video)
Sensor size	1″, 20 million effective pixels		1/2.3″, 12.4 million effective pixels
Field of view	77°		94°
Lens length	38 mm		20 mm
Image size	5472 × 3648 pixels		4000 × 3000 pixels
Video size collected	4 k (3840 × 2160 pixels)		4 k (3840 × 2160 pixels)
Maximum flight time	31 min		28 min
GPS accuracy	Vertical	±0.5 m	±0.5 m
	Horizontal	±1.5 m	±1.5 m

Environmental variables that may affect the detectability of underwater forage fish from RPAS imagery were first identified from the literature [4,5,21–23,32], and recorded for each sample. The variables included in our analysis were: wind speed, cloud cover, sun altitude, and secchi depth (Table 2). Through the literature review, different classes of each environmental variable were identified (Table 3). No definitive thresholds were identified for secchi depth for two reasons: the literature recommended avoiding highly turbid waters rather than suggesting specific thresholds, and the secchi depth that is required to see a subsurface target depends on other factors (e.g., target depth, color, and size, and other environmental conditions [22,23,25,29,32,33,43]. The statistical analysis used the recorded values (i.e., no transformations were applied) for all the variables except secchi depth, which was corrected for the observed sun angle using equations from [44] to minimize the combined effects of turbidity and sun altitude variability.

Table 2. The environmental variables considered in the analysis and recorded for each sample.

Environmental Variable	**Collection Method**
Wind speed (km/h)	In field, with hand held anemometer.
Sea state (cm)	In field, visual estimation of wave height and texture (glassy, ripples, waves) according to Beaufort classification.
Cloud cover (%)	In field, visual estimate of percent cloud cover.
Sun altitude (°)	After field work, sun angle calculator calculated from location and time of survey [45].
Secchi depth (m)	In field, maximum depth a standard 20 cm secchi disk is visible, a proxy for water turbidity.

Table 3. The classes of each environmental variable and suitability for collecting marine aerial imagery summarized from a literature review.

Variable	Thresholds	Classification	Rationale	References
Sun altitude	<25°	Moderate	Low angles reduce solar irradiance and illumination [22]. found high to moderate mapping confidence of subsurface habitat features from sun angles from 6.5–40°.	[21,22,32]
	25–40°	Optimal	Moderate angles have enough solar irradiance for correct illumination while mitigating sun glint.	
	>40°	Suboptimal	High angles increase sun glint for nadir surveys.	
Cloud cover	≤10%	Optimal	Best conditions with an optimal sun angle in order to have lots of light to illuminate subsurface features. Consistent reflectance and radiometry across survey.	[22,28,32]
	>10, <90%	Suboptimal	Worst conditions due to irregular patterns of bright cloud reflectance.	
	≥90%	Moderate	Consistent reflectance and radiometry. Specular reflectance of the clouds occurs on the surface of the water and obscures benthic features.	
Wind speed	≤5 km/h	Optimal	No wind ripples were observed.	[22]
	>5 km/h, ≤8 km/h	Moderate	High confidence was achieved in winds up to 8 km/h. Wind speeds 5–8 km/h may cause wind ripples depending on the angle of the sun.	[22,33]
	>8 km/h	Suboptimal	Wind ripples were observed at wind speeds greater than 8 km/h.	[22]
Sea surface	Beaufort class 0 (glassy)	Optimal	Sea surface is mirror-like but not necessarily flat [46]. This Beaufort category corresponds to optimal wind speed (≤1 km/h).	[22]
	Beaufort class 1 and 2 (ripples-waves)	Moderate	Class 1 is characterized by ripples without foam crests with winds from 1–5 km/h, while class 2 is characterized by small wavelets with crests that do not break and winds from 6–11 km/h [46]. As such, these classes correspond to optima, moderate and suboptimal classes of wind. Ref. [23] found decreasing sighting rates of marine organisms in worsening sea surface conditions. Most aerial marine surveys occur during Beaufort classes < 3.	[19,21,23]
	≥Beaufort class 3 (waves)	Suboptimal	Includes classes characterized with large wavelets with breaking peaks (Class 3) and rougher with winds of 12 km/h or greater [46].	[19,21,23]

2.3. Imagery Analysis

The visual analysis of RPAS imagery consisted of an experienced viewer counting all visible lures identified in the video at each depth. In order to standardize the process, all sample videos were watched on a 4 k screen in a dark room by a solitary, experienced viewer, following methods by [19]. The video was paused, slowed, and zoomed into if there was any uncertainty in lure detection to decrease perception errors [23,25]. Perception errors occur when targets are misclassified or missed entirely by the viewer, even though they are available to be seen [23,25,26].

2.4. Statistical Analysis

The dataset produced from the imagery analysis includes counts of each fish lure at each depth and associated environmental variables (Table 1) that occurred during data acquisition. The number of identified lures in each video (lure count) were divided by the total number of lures that were present in the video (n = 10 for each lure type) to produce a percentage metric called "lure visibility". The three replicates recorded for

each sample were averaged, and the standard deviation used as metrics of precisions of lure identification.

After data organization, a statistical analysis was performed to compare the lure visibility to the environmental conditions in order to identify the optimal conditions for highly accurate forage fish detections. The statistical analysis consisted of two steps. Firstly, the environmental data were used in a cluster analysis, independent of the lure visibility data, to group environmental conditions. The lure visibility was compared between the different clusters to define environmental thresholds for optimal or suboptimal conditions. The clustering analysis method employed a *k*-means cluster algorithm [47] to group the data by considering wind speed, wave height, cloud cover, sun altitude, and secchi depth. The number of clusters (*k*) was chosen manually based on the elbow method, which allows the user to see and select the number of clusters that reduces the within sum of squares while balancing the need for minimal clusters for reduced complexity [47].

Secondly, a principal components analysis (PCA) and Spearman's correlation analysis were conducted to determine which specific environmental variables had the most impact on lure visibility at each depth. There were four PCA's completed for these data, one for each depth. In order to use the PCA, the data first needed to be scaled to ensure there were no zeros in the dataset [47]. Additionally, lure visibility was compared to each environmental predictor variable using Spearman's ρ_s to determine the strength, direction, and significance of relationships. Spearman's rank correlation was chosen as it can measure the strength and direction of all types of monotonic relationships and is appropriate to use when data are non-normal with outliers [48]. All data analyses were preformed in R software version 1.3.1073 [49], including the stats package for the cluster analysis [50] the ade4 package for the PCA analysis [51], and the corrplot package for the correlation analysis [52].

3. Results

3.1. Sampled Environmental Conditions

A total of 127 experimental samples were recorded during summer 2021 covering different environmental conditions. Since the environmental conditions were sampled opportunistically, they were not equally sampled across their ranges and their distributions contained outliers (Table 4). Broadly, sun altitude was relatively evenly sampled with a range from 8° to 55°, while cloud cover, due to its non predictable nature, had more samples in overcast (≥90–100%, n = 72) than clear conditions (≤10%, n = 37) or mixed conditions (>10, <90%, n = 18). Similarly, the wind and wave conditions had unevenly sampled categories, with low winds (<5 km/h, n = 116) and glassy seas (0 cm, n = 81) dominating relative to wind speeds above 5 km/h (n = 11) and samples with ripples or waves (n = 46). Finally, secchi depths were no shallower than 4.4 m, and had low variability (standard deviation of 0.6 m).

Table 4. The descriptions of sample distribution for each environmental variable including descriptive statistics and the number of samples in each category defined by the literature (Table 3). The one exception was the equal interval classification for secchi depth as there were no thresholds seen in the literature regarding secchi depth. The descriptive statistics chosen included mean, standard deviation (SD), and range.

Variable	Descriptive Statistics		Classes in Literature	Number of Samples in Each Class
Sun altitude	Mean	30.38°	<25°	50
	SD	13.52°	25–40°	40
	Range	8.20°, 54.53°	>40°	37
Cloud cover	Mean	65%	≤10%	37
	SD	43%	>10, <90%	18
	Range	0%, 100%	≥90%	72

Table 4. *Cont.*

Variable	Descriptive Statistics		Classes in Literature	Number of Samples in Each Class
Wind speed	Mean	1.6 km/h	≤5 km/h	116
	SD	2.4 km/h	>5, ≤8 km/h	8
	Range	0.0, 11.1 km/h	>8 km/h	3
Wave height	Mean	0.7 cm	Glassy	81
	SD	1.5 cm	Ripples	40
	Range	0, 10 cm	Waves	6
Adjusted secchi depth	Mean	5.2 m	4.4–5.4	100
	SD	0.6 m	5.5–6.4	26
	Range	4.4 m, 7.5 m	6.5–7.5	1

3.2. Summary Statistics on Lure Visibility

The resulting summary statistics (Table 5) show broad patterns in reduced visibility with lure depth, lure size, and based on lure color. Lure A (dark lure) had lower average visibility at all depths than any silver lure (lure B, C, D), and lure visibility decreased and became more variable with increased depth. The one exception to this was lure A which had a lower standard deviation at 2.0 m than at 1.5 m because this lure was almost never visible at 2.0 m depth (Table 5). In addition, lure A had greater variation in visibility (larger standard deviations) at most depths than the other lures with the exception of lure C having a larger standard deviation at 2.0 m. This is likely due to the same reason that lure A was almost never visible at this depth. Furthermore, for lures B, C, and D, visibility decreased with lure size.

Table 5. Mean and one standard deviation ("SD") of visible lure counts recorded for lures at each depth, independent of the other environmental conditions. Lure visibility can be inferred from this table as well as it can be calculated by dividing the mean and standard deviations by the total number of each lure.

Lure	Lure Description			0.5 m		1.0 m		1.5 m		2.0 m	
	Size	Color	Total Number of Lures	Mean	SD	Mean	SD	Mean	SD	Mean	SD
Lure A	10 mm	Dark	10	9.48	1.39	5.33	3.75	2.27	3.51	0.56	2.11
Lure B	11 mm	Silver	10	10	0	10	0	9.98	0.20	9.82	0.98
Lure C	9 mm	Silver	10	10	0	10	0	9.92	0.48	9.43	1.74
Lure D	5 mm	Silver	10	10	0	10	0	9.87	0.68	9.02	2.18
All lures			40	39.48	1.52	35.32	3.76	31.72	3.64	28.32	6.05

Additionally, the mean and standard deviations of specific lures at specific depths show the effect of the sampled environmental conditions on lure visibility. For example, lures B, C, and D were all visible (mean of 10) with no variability (standard deviation of 0) at 0.5 m and 1.0 m, meaning that none of the environmental conditions sampled in this research impacted their visibility at these shallow depths. Contrasting this, lure A was almost never visible at 2.0 m depth showing that very specific conditions may be required to detect this lure at 2.0 m depth.

3.3. Relationship between Environmental Conditions and Lure Visibility

The resulting relationships between the environmental conditions and the lure visibility are first reported through the cluster analysis results and followed by the PCA and Spearman's correlation analysis. The overall trends from all three analyses showed that each lure type (dark lure vs. silver lures) was affected by different environmental variables.

The results of the *k*-means cluster analysis of the environmental variables produced 5 distinct clusters (Table 6). Cluster 2 ($n = 11$) was associated with high winds (1.5–11.1 km/h), ripples and waves (3–10 cm), moderate to high sun angles (32–55°), mixed and overcast

cloud coverage (>50%), and relatively shallow secchi depths (4.4–5.3 m). Cluster 1 (n = 32) encompassed similar conditions but with lower wind (<7.0 km/h) and ripples (<2 cm). Environmental conditions comprising Cluster 3 (n = 32) had optimal conditions with calm winds (0 km/h), glassy seas (0 cm), and clear skies (<5%). Cluster 4 (n = 44) had overcast (>95%), low-moderate wind (<5.5 km/h), glassy seas (wave height 0 cm), and low-moderate sun angles (5–40°), with a moderate secchi depth (4.8–5.6 m) while Cluster 5 (n = 8) had similar environmental conditions, except for a broader range of cloud cover conditions (0–100%), calm wind (0.0 km/h), glassy seas (wave height 0 cm) and the lowest water turbidity (6.4–7.5 m).

Table 6. The range of each environmental variable in each cluster.

Environmental Variable	Cluster 1	Cluster 2	Cluster 3	Cluster 4	Cluster 5
Cloud cover	>50%	>10%	<5%	>95%	0–100%
Wind speed	<7.0 km/h	1.5–12.0 km/h	0.0 km/h	<5.5 km/h	0.0 km/h
Wave height	<2 cm	3–10 cm	0 cm	0 cm	0 cm
Sun altitude	32–55°	38–53°	10–55°	8–40°	8–37°
Adjusted secchi	4.4–5.3 m	4.4–5.6 m	5–5.5 m	4.8–5.6 m	6.4–7.5 m

The different sets of environmental variables represented by each cluster were compared to lure visibility at each depth to detect broad trends of optimal and suboptimal conditions (Figure 3). At 0.5 m depth, the dark lure (lure A) visibility was the lowest in Cluster 5. However, at 1.0 and 1.5 m, this lure was most visible in the only cluster with clear sky conditions (Cluster 3), while the other clusters had similar counts. As for the silver lures (lures B, C, and D), had reduced visibility happened at 1.5 and 2.0 m and occurred only in the two clusters with elevated wind and wave height conditions (Cluster 1 and 2). Lastly, lure visibility decreased with depth and increased with lure size, reflecting the results of the summary statistics.

The PCA analysis was completed separately for each specific depth, considering the four different lures (A B, C, and D) and the environmental conditions. The results show that the PCA and correlation analysis for 0.5 m and 1.0 m depths excluded the three silver lures (lures B, C, D) because these lures were always 100% visible and did not contribute any variability to the PCA (Table 5). This means none of the sampled environmental conditions impacted the visibility of lures B, C, or D at these shallow depths. Similarly, lure A was excluded for the 2.0 m PCA analysis. However, in this case, within the environmental conditions that were sampled, this lure was almost never visible (Table 5).

At 0.5 m and 1.0 m, visibility of the lure A) contributed greatly to the PCA (Figure 4), meaning that the variation in lure A visibility was well represented by the first two principal components. At both depths, lure A's vector arrow was opposite to cloud cover (Figure 4), suggesting a negative relationship (i.e., as cloud cover increases, visibility of lure A will decrease). Lure A's vector was not close to any other variables, suggesting that lure A's visibility does not have a positive relationship with any environmental variables.

At 1.5 m, lure B, C, and D visibility showed the strongest contribution to the PCA while lure A contributed less (Figure 4). Lure A showed a positive relationship to secchi depth and a negative relationship to cloud cover. The positive relationship to secchi depth suggests that lure A was more visible in less turbid water. Lures B, C and D. However, show positive relationships to each other and negative relationships to wind speed, wave height, and sun altitude.

This pattern was similar at 2 m depth with lure B, C, and D having the highest contribution value to the PCA, positive relationships to each other, and negative relationships to wind speed and wave height.

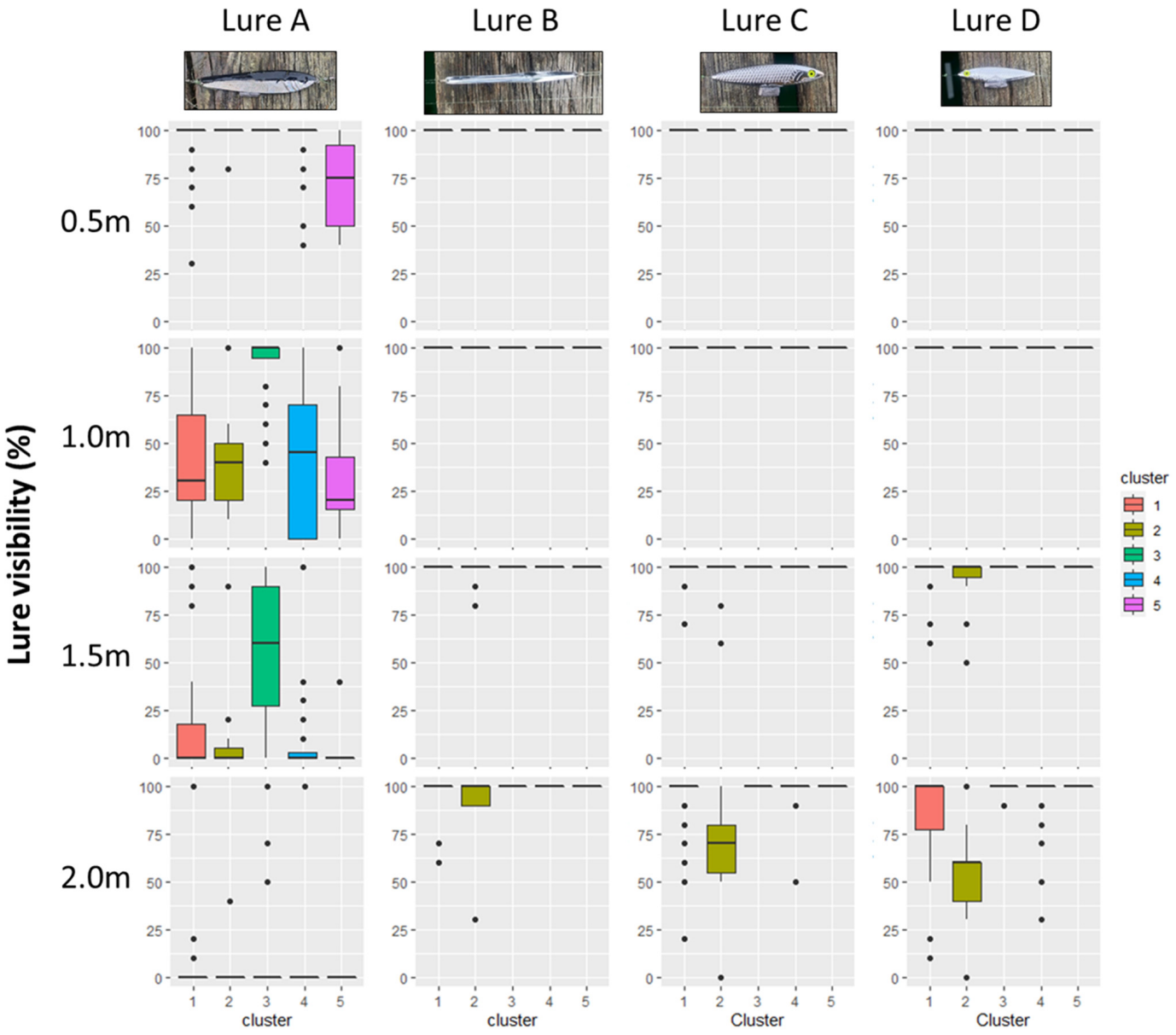

Figure 3. The lure visibility in each cluster at each depth summarized for all experimental samples. The top and bottom of the boxes represent the first and third quartiles, while the black bar in the middle of the box represents the median. The whiskers at either end of the box show where 95% of the data fall. The black dots represent outliers that fall outside of the 95% confidence interval. Note that when there is only a black bar and no box or whiskers, it shows that there is either 100% or 0% visibility.

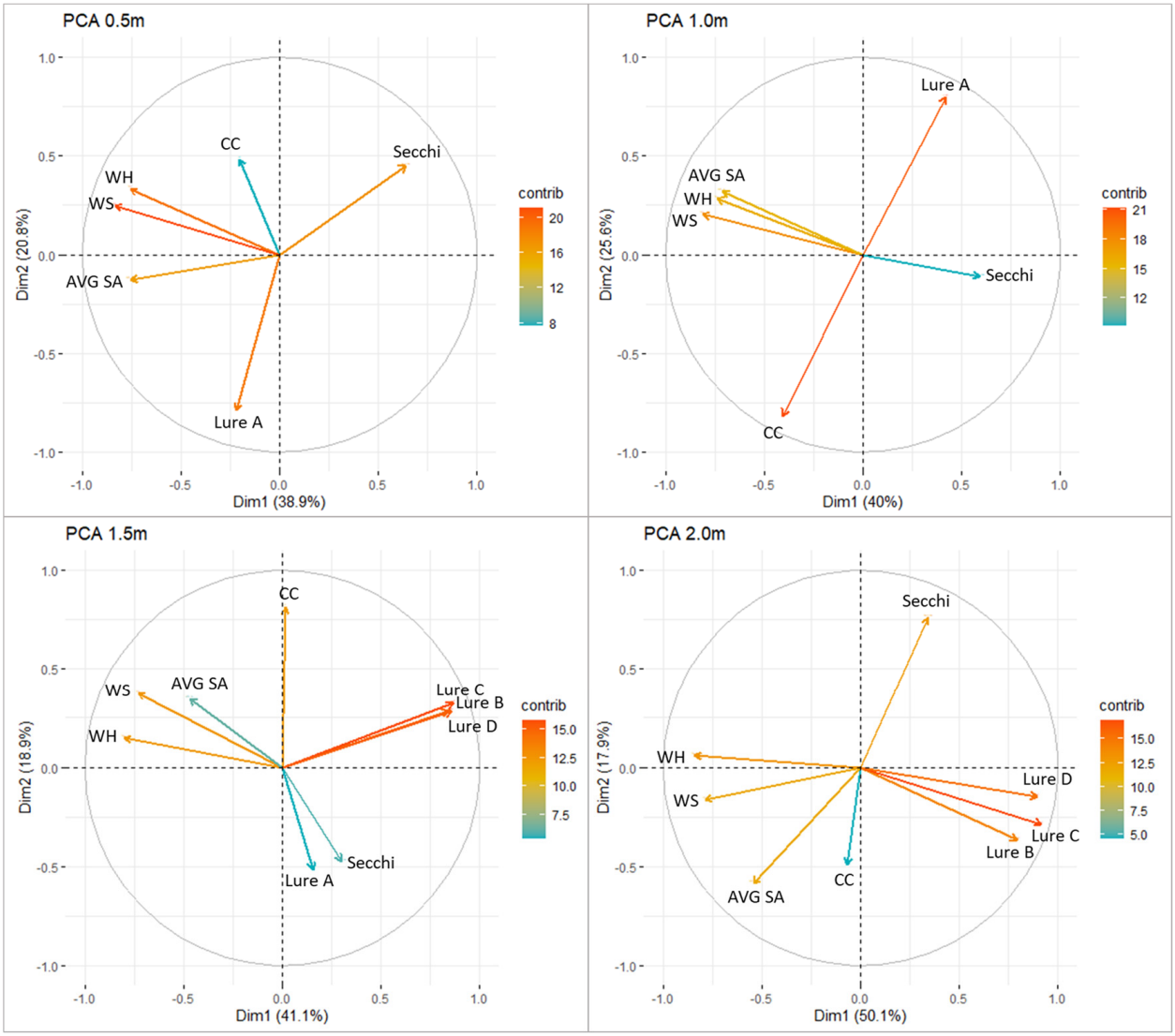

Figure 4. The contribution of each variable to the first two principal components for each depth's PCA is displayed by the length and color of the arrows. The variables shown here are cloud cover (CC), wave height (WH), wind speed (WS), sun altitude (AVG SA), secchi depth (Secchi), and lure visibility for each lure (Lure A, Lure B, Lure C, Lure D). The variables are represented by arrows whose color and length corresponds to how much variability they account for (i.e., how much they contribute) to each PCA. Variables that are opposite to each other are negatively correlated and those that are close together are positively correlated. The two dimensions displayed are the first and second principal components of each PCA. The values associated with each dimension are the eigenvalue associated with the principal component.

Spearman's correlation analysis showed similar relationships to the PCA (Table 7). The lures that were excluded from the PCA at 0.5 m, 1.0 m, and 2.0 m PCA were also excluded from this correlation analysis for the shared reason of having no variability in their visibility. Firstly, lure A showed somewhat similar patterns to those expected based on the results of the PCA (Figure 4). At 0.5 m, lure A showed a weak negative correlation with cloud cover. At 1.0 m, lure A showed a strong relationship with cloud cover and a weak positive relationship secchi depth. At 1.5 m, lure A continued to display a strong relationship with cloud cover, but additionally showed a weak negative correlation with wave height and wind speed (Table 7). Lures B, C, and D displayed correlations to all of the environmental variables (Table 7). At 1.5 m, all three lures showed weak negative relationships with wave height, wind speed, and sun altitude except for lure D which showed a moderate

relationship with wind speed and a weak positive correlation with secchi depth. At 2 m, all the silver lures displayed moderate negative relationships with wind speed and sun altitude. Additionally, lure C and D displayed strong negative relationships with wave height while lure B showed a moderate negative relationship. Lure C and D also showed a weak positive relationship with secchi depth and lure D displayed a weak negative relationship with cloud cover (Table 7).

Table 7. Significant Spearman's correlations (ρ_s) between the variables included in each PCA ($p < 0.05$). The red cells indicate positive relationships, blue cells indicate negative relationships, and empty cells display non-significant relationships. The silver lures were not included at 0.5 m and 1.0 m because always visible and similarly the dark lure was excluded for 2 m because it was almost never visible.

Depth	Lure Name	Lure Color	Secchi Depth	Cloud Cover	Wave Height	Wind Speed	Sun Altitude
0.5 m	A	Dark		−0.18			
1.0 m	A	Dark	0.26	−0.65			
1.5 m	A	Dark		−0.54	−0.20	−0.18	
	B	Silver			−0.25	−0.24	−0.19
	C	Silver			−0.30	−0.26	−0.19
	D	Silver	0.19		−0.29	−0.32	−0.25
2.0 m	B	Silver			−0.37	−0.34	−0.21
	C	Silver	0.19		−0.55	−0.48	−0.38
	D	Silver	0.28	−0.18	−0.52	−0.44	−0.39

3.4. Optimal and Suboptimal Conditions

All of the environmental variables were shown to impact the visibility of a lure type, depending on lure color, size and depth. The silver lures (lures B, C, and D) visibility was most impacted by wind speed and wave height, followed by sun altitude while the dark lures (lure A) visibility was most impacted by cloud cover (Table 8). Specifically considering each environmental variable, optimal and suboptimal ranges or thresholds were identified based on the results of the statistical analysis combined with consultation of the literature on marine aerial imagery surveying (Table 3). In order to make the recommendations practical for increased accuracy in RPAS forage fish surveys, conservative thresholds were chosen as the forage fish seen in RPAS surveys will likely be less visible to the imagery analysist than the stationary lures in the model fish school. Table 8 summarizes the thresholds for the environmental conditions that should be considered to minimize detections errors in forage fish surveys for fish species that share similar color scheme represented here.

Table 8. The recommendations for conditions to target (optimal) and avoid (suboptimal) for RPAS forage fish surveys based on the two lure types.

	Condition Description	Thresholds
	Dark lure	
Optimal	Clear skies	Cloud cover <10%
Suboptimal	Mixed and overcast skies	Cloud cover >10%
	Silver lures	
Optimal	Glassy seas	Wave height 0 cm
	Calm winds	Winds < 5 km/h
	Low—moderate sun altitude	Sun altitude 20–40°
	Low turbidity	Secchi depth > 5 m

Table 8. *Cont.*

	Condition Description	Thresholds
Suboptimal	Ripples and waves	Wave height > 1 cm
	Moderate—strong winds	Wind speed > 5 km/h
	High sun altitude	Sun altitude < 20°, >40°
	High turbidity	Secchi depth < 5 m

4. Discussion

The objective of this study was to determine environmental conditions that are optimal and suboptimal for detecting surface schools of forage fish in RPAS imagery. The analysis was conducted based on RPAS imagery acquired over a model fish school with dark and silver lures of different sizes, positioned at different depths, and considering natural environmental conditions in the spring/summer coastal waters of BC, Canada. Clear skies, low winds, glassy seas, moderate sun angles, and low turbidity, generally allowed for the highest visibility for all the lures (Table 8). However, specific conditions, including wind speed, wave height, sun altitude, and turbidity impacted the visibility of the silver lures (lures B, C, D) the most, while the dark lures visibility (lure A) was most impacted by cloud cover (Figures 3 and 4; Tables 7 and 8). Furthermore, as expected, the dark lure was less visible than the silver lures, smaller lures were less visible than larger lures, and visibility decreased with lure depth. Targeting the optimal conditions in Table 8 should minimize availability bias in RPAS forage fish surveys caused by poor conditions making forage fish schools unavailable for detection.

This discussion first focuses on the optimal and suboptimal conditions recommended for RPAS forage fish surveys (Table 8), followed by the effect of lure color, size, and depth on visibility and lastly discusses of the practical application of RPAS to map forage fish.

4.1. Environmental Conditions

Among the identified conditions, wind speed and wave height (highly correlated to each other) had the largest impact in silver lure visibility with thresholds of <5 km/h and 0 cm (i.e., glassy), respectively, as optimal for RPAS data acquisition. At glassy seas conditions, target distortions are minimized as there is less light refraction (Figure 5A–C,E) compared to higher wind and wave conditions (Figure 5D,F). Additionally, the interaction of waves with sunlight may cause sun glint (Figure 5F) and cloud glare (Figure 5C,D) [33,53]. The strong contribution to the PCA (Figure 4) and the moderate to strong negative correlation with lures B, C, and D at 1.5 m and 2.0 m (Table 7) show the importance of these two variables to the silver lure visibility. These conditions were the most important for silver lures located at 1.5 and 2.0 m where the visibility was higher when there were low winds and glassy seas (Table 7, $0.24 > \rho_s > -0.55$). These lures were often visible at these depths (Table 5) but had the lowest visibility in the only clusters that had elevated sea surface/wind conditions (Clusters 1 and 2 in Table 6 and Figure 3), illustrating that rough conditions are particularly important to avoid in order to ensure visualization of these lures at these deeper depths. Lastly, Cluster 4 had winds up to 5.5 km/h but did not have elevated wave heights or reduced lure visibility, suggesting that winds up to 5.5 km/h may not cause surface waves that impact lure visibility (Table 6). Even though we were only able to sample wind speeds up to 11.1 km/h and wave heights up to 10 cm (Table 4), it is still clear that the rough sea surface conditions provided suboptimal conditions for detecting the lures.

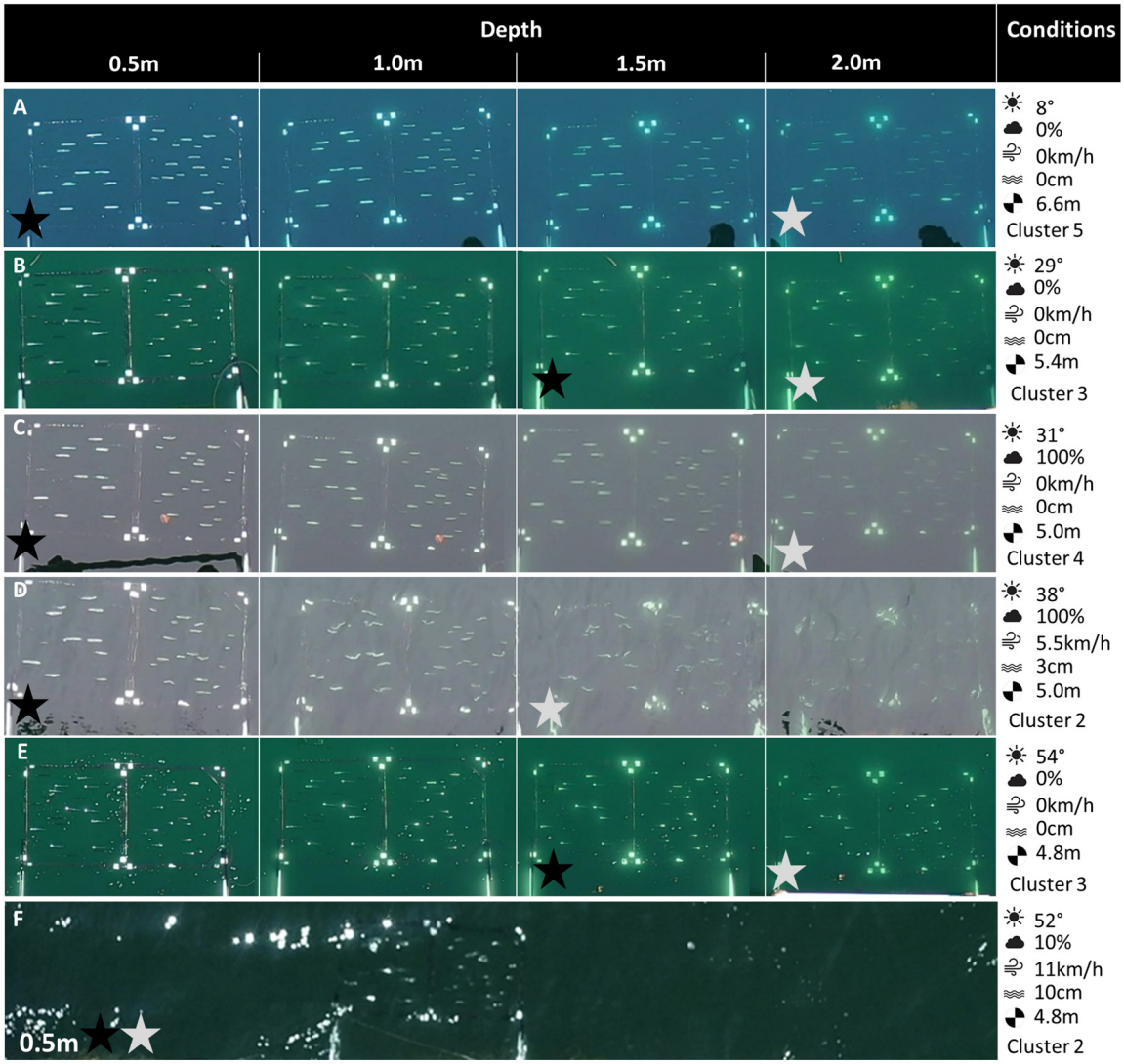

Figure 5. Screenshots of video samples to show how the model fish school visually appears in different environmental conditions. These screenshots are taken from the perspective of the drone looking down at the model fish school. Panels (**A**–**F**) show examples of the model fish school at different depths (columns) in different conditions. The conditions are listed on the right side of each row in the order of sun altitude (°), cloud cover (%), wind speed (km/h), wave height (cm), and secchi depth (m) along with the cluster that each sample is in. The black and gray stars show which depth the dark and silver lures start to disappear at, respectively. Panel F only includes one depth (0.5 m) as the lures were not visible at any other depth and to show how sun glitter across the frame impacts looks similar to the silver lures. Note the resolution of the imagery illustrates the detail captured by the RPAS imagery at 15 m height. Note the different colors of the water are due to the different environmental conditions during imagery acquisition.

Most RPAS studies recommend a larger range of wind speeds and wave heights usually with a maximum threshold of 8–11 km/h and 0.5 m wave height. However, these studies usually target marine megafauna or benthic habitat which are much larger than forage fish [21–23,32]. The most conservative findings from [22] justify the relatively low thresholds of glassy seas and 5 km/h, as the authors found that winds between 5 and 8 km/h may produce wind ripples. Note the distortions of the silver lures in Figure 5D due to the wind ripples compared to the undistorted shape of the lures in panel C with calm winds and glassy seas (and otherwise similar conditions).

Sun altitude was the second most important environmental variable for silver lures (lure B, C, D) visibility. The sun angle altitude was negatively correlated with visibility of lures B, C, and D at 1.5 and 2.0 m depth (Table 7, $-0.39 > \rho_s > -0.19$), meaning that the higher the sun altitude (i.e., close to nadir), the lower the ability to identify silver lures. The optimal range for sun altitudes between 20° and 40° balances the need for adequate solar irradiance to illuminate forage fish targets and avoid sun glint on the surface. Solar altitude is important, as a minimum amount of solar irradiance is required to adequately illuminate targets for visual identification [22,31,43] associated with the light attenuation properties of the water constituents, the characteristics of the target (e.g., color, size, depth in the water column), and the contrast between the target and the background [33]. Higher solar altitudes will deliver more solar irradiance. However, at these angles sun glint may happen preventing optimal visualization of subsurface features [33]. These suboptimal sun glint conditions are a result of sun light interacting with ripples and waves to cause an effect called "sun glitter" (Figure 5F) [5,19,33]. Sun glitter is known to cause errors in classification of subsurface features [30] and should be avoided in RPAS forage fish surveys as it is a source of false-positive detection errors.

Considering the sun glitter constraint, the minimum recommended sun altitude of 20° reflects the negative correlation between sun altitude and lures B, C, and D, the high visibility of lures B, C, and D in clusters that had low minimum sun altitudes, and results in the literature. Firstly, lures B, C and D visibility was negatively correlated with sun altitude at 1.5 and 2.0 m depth (Table 7). Secondly, there was no reduced lure B, C, or D visibility in clusters with low altitudes of 8° and 10° (Cluster 3, 4, and 5 in Table 6 and Figure 3). Lastly, minimum solar altitudes seen in the literature are generally in a range of 25–30°. However, some research suggested that lower altitudes may provide adequate illumination [22,28,31,32]. Authors from [28] found that the minimum 30° angle recommended for piloted aerial benthic habitat surveys from [32] offered more than sufficient light to illuminate benthic eelgrass vegetation. Additionally, [22] detected eelgrass with high confidence down to the lowest sun altitude sampled of 6.5°. They thought that low altitude RPAS flights may have lower minimum sun angle requirements because the sensor is closer to the target than to the pilot in higher altitude piloted aircraft surveys [22]. The results from [33] that found a significant decline in solar irradiance below 20–25° supported the minimum 20° threshold.

The maximum recommended solar altitude of 40° is based on the reduced visibility of lures B, C, and D in the clusters with the highest sun angles (Clusters 1 and 2 in Figure 3) and the consistent negative correlation between sun altitude and silver lure visibility at 1.5 m and 2.0 m depth (Table 7). Given the glassy sea surface that is recommended for forage fish surveys (Table 8), the threshold of 40° should avoid sun glint for cameras with the common 94° field of view and a nadir sensor angle [32,33]. Sun glint was never observed on the water's surface directly above the model fish school (i.e., blocked the model fish school from imagery viewer) during glassy sea surface conditions. However, sun glint was observed near at the edge of imagery frames recorded in glassy seas conditions with sun altitudes above 43°. While there was no sun glint directly blocked visualization of the model fish school in any video sample (Figure 5E), glint was observed at the edges of the imagery with glassy conditions at angles above 43°. Upper thresholds found in the literature were either 40° or 45° for the same rationale of avoiding sun glint [4,22,28,30–32].

Secchi depth was shown to be somewhat important to lures A, C, and D seen in the weak positive correlations at 1.0, 1.5, and 2.0 m depths (Table 7) and the reduced visibility of lures B, C, and D at 2.0 m in the clusters with the shallowest secchi depths (Clusters 1 and 2 in Figure 3 and Table 6). The negative relationships between secchi depth and lure visibility (Table 7, $0.19 > \rho_s > 0.28$) make sense as deeper secchi depths suggest less turbid waters and increased ability to detect subsurface targets. Secchi depth likely did not show stronger relationships with lure visibility because the shallowest secchi depth recorded was at least 2.4 m deeper than the model fish school and the samples did not capture a wide range of secchi depth conditions (Table 4).

Secchi depth acts as a proxy for turbidity, which controls light attenuation in the water column and results in less light available to illuminate deeper targets and can be a large contributor to availability errors in aerial marine surveys [24,25,53–55]. Light is absorbed and scattered by particulate matter in the water column, causing a gradual decrease in available light and a gradient of diminishing visibility [33,56]. As such, it is difficult to identify a meaningful secchi depth threshold for the practical application of RPAS to survey forage fish as forage fish schools encountered in surveys will likely be at different depths than tested in this experiment. However, our results suggest that a secchi depth no less than 5 m should maximize lure visibility up to 2 m depth.

Lastly, cloud cover had the largest impact on the visibility of lure A. This importance was shown by strong contribution of cloud cover and lure A visibility in the 1.0 m PCA (Figure 4) and the strong negative correlation to lure A at 1.0 m and 1.5 m depths (Table 7; $-0.65 > \rho_s > -0.54$). Additionally, the cluster analysis had the highest visibility of dark lure counts in the only cluster with clear conditions (Cluster 3 in Figure 3 and Table 6). Clear skies maximize solar irradiance available to illuminate subsurface targets and minimize the negative effects that specular cloud reflectance can have on the surface [21,28,30,33,53]. This is well illustrated by the difference in lure A visibility in panels B and C in Figure 5. Panel C has overcast conditions and lure A is difficult to see at 0.5 m, where as panel B has similar conditions with the exception of clear skies, and lure A is difficult to detect at 1.5 m. The results from the cluster analysis, PCA, and correlation agreed with the recommended clear sky condition from the literature for marine aerial imagery surveys.

4.2. Lure Color, Size and Depth

The dark lure was less visible than the silver lures, and visibility decreased with size within the three silver lures, and visibility decreased with depth (Table 5). Lure A was less visible than lures B, C and D (Table 5) likely because lure A had lower contrast with the standardized dark water column background. Contrast between the target and the background in aerial imagery is an important factor impacting the detectability of targets [23,29,30,32,57,58]. Contrast in imagery is a function of the light available to illuminate the targets at a given depth and the visual appearance of target and the background [29,33]. However, the type of background habitats encountered in RPAS forage fish surveys of shallow nearshore habitats will provide varying degrees of contrast for each detection type. For example, Shiner Perch (represented by the dark lure) detected in our RPAS forage fish survey imagery was very obvious over light sand bottom types due to the high contrast (Figure 6). In this research, these conditions are not considered given that the background was always a deep water column.

Lure size had a negative relationship with visibility within the three silver lures (lures B, C, and D; Table 5). This is likely an impact of the reduced ground sampling distance (GSD) and the reduced visual ability to detect the small targets depth. The ability to detect targets in imagery is highly dependent on the GSD (i.e., distance between two pixels' centers measured on the ground) [21]. Additionally, it was more difficult to visually identify the smaller targets at deeper depths as the edges of the smallest lure were the first to blur into the background and this was likely due to environmental factors affecting surface texture that would alter the shape of the lures (Figure 5) and variables that would limit contrast (turbidity, sun altitude, cloud cover). The effect of contrast and size is obvious from the difference between the minimum secchi depth and the maximum lure depth. Lure B (largest silver lure) disappeared at 1.5 m and 2 m in some conditions while the secchi depth was always visible to at least 4.4 m (2.4 m deeper than the lures; Figure 5). Lastly, lure visibility decreased with lure depth (Table 5). This is due to diminishing light levels available at deeper depths to illuminate targets for correct identification as previously discussed.

Figure 6. Image of Shiner Perch schools over sand from an RPAS forage fish surveys. There are ~50 fish in the red circle.

4.3. Practical Application and Future Directions

False negative detections caused by poor conditions are difficult to model or factor into data, so targeting environmental conditions for RPAS forage fish surveys that will minimize these errors is very important for accurate forage fish quantification [24,26,59,60]. The suboptimal conditions (Table 8) should be avoided, and if they cannot, they need to be recorded during field imagery acquisition so potential sources of error in the type of forage fish schools can be better understood [32].

Some of the environmental conditions such as sun angle and tides can be easily predicted and therefore planned around. However, others cannot, thus requiring user flexibility and local knowledge to optimize survey potential for forage fish. For example, turbidity is not always predictable. However, usually it is greater after stormy events, on rising tides, and during phytoplankton blooms, and during periods of significant freshwater input in coastal areas [21,29,32]. Local knowledge of seasonal changes in water clarity should be used to plan surveys [32]. Cloud cover and wind can somewhat be predicted with short term (e.g., 3–5 days) local marine and weather predictions [32]. Field days in Barkley Sound for example were planned to avoided July and August as these months are known to have foggy mornings and a high probability of a phytoplankton bloom (Personal Communication, Jennifer Yakimishyn, June 2020). Field days also targeted mornings which are known to be less windy and ultimately less wavy in coastal areas in summer. Planning forage fish surveys requires logistical flexibility so that conditions can be evaluated on each planned field day and adapted or rescheduled if needed [32].

In addition to environmental conditions, planning of RPAS surveys should also consider the seasonal timing of forage fish use of nearshore areas and their depth in the water column based on specific species life histories. In this study we found that visibility is positively related to fish size and negatively related to their depth. As such, RPAS surveys should be used during months when forage fish are largest and most visible to the RPAS near the sea surface. For example, RPAS surveys targeting Sand Lance should occur in late summer and early fall when the young-of-the-year are larger than during the spring and they spend more time foraging in large schools in the upper water column before they burry in subtidal sand for winter [36,61]. An important consideration is evaluation of detection of false negatives caused by poor conditions. These are difficult to model or factor into our dataset, so targeting environmental conditions for RPAS forage fish surveys that will minimize these errors is very important for accurate forage fish quantification [24,59,60].

The differences between the lures used in this experiment and forage fish encountered in RPAS surveys should be considered in the practical application of these results. The factors that will add complexity to detecting forage fish in RPAS imagery will likely include the unknown locations of forage fish schools to imagery analyst and the effect of moving targets. Forage fish schools in RPAS imagery will likely be harder to detect than the model fish school because the imagery analyst will not know where the forage fish schools are, in contrast with the model fish school and fish lures used in this experiment. Additionally, forage fish are moving targets in contrast with the stationary lures used here. Movement will likely aid in their visual detection as movement should help differentiate forage fish from stationary benthic background features in imagery. This rationale is based on the recommendations for video imagery to capture movement in the literature [1,23,43] and the 2020 test surveys where forage fish movement captured in RPAS video imagery was necessary to detect many fish schools, particularly those identified with fish flash detections.

Lastly, applying and testing the recommendations for optimal conditions on RPAS forage fish surveys may help develop correction factors for false negative errors in order to make forage fish population estimates from RPAS surveys. There is a growing body of literature that aims to understand availability and perceptions errors with a goal to make population estimates from aerial surveys by estimating correction factors [23–26,62]. In this study, optimal conditions are recommended to minimize the availability error for forage fish caused by poor conditions of cloud cover, sun altitude, wind speed, wave height, and turbidity. However, understanding additional variables that will influence availability and perception errors and be present in RPAS forage fish surveys is needed before correction factors can be made to make forage fish population estimates from RPAS surveys. Such variables will likely include vertical distribution of forage fish in the water column, school size, background type (and contrast as previously discussed), and fish behaviour [23–26,62].

5. Conclusions

Through our experiments at two coastal Vancouver Island nearshore locations, optimal environmental conditions for detecting the fish lures in RPAS imagery were defined. As the lures in this experiment were generalized based on forage fish color, size and counter-shading, the results provide a guideline for optimal conditions for detecting forage fish in RPAS surveys. Low surface winds, glassy seas, moderate sun angles, low turbidity and clear skies allowed for the highest lure visibility and are the recommended environmental conditions to ensure accurate forage fish surveys. However, further research is required to field test these recommendations on specific forage fish species, and to further develop protocols specific to RPAS surveys of forage fish. Forage fish visibility in RPAS forage fish surveys will likely depend on additional site-specific variables such as differentiating seabed substrate background types (e.g., eelgrass, light sand) and the contrast they provide to forage fish water column detection and school metrics such as school density and size. An additional consideration for further defining this protocol should note that forage fish schools may occur and be visible at deeper depths than tested in this research, and could be combined simultaneously with acoustic sampling methods. Overall, RPAS provides a practical, non-invasive method to capture information on schooling forage fish species in nearshore waters of coastal regions.

Author Contributions: Conceptualization, all authors; field work, N.R.H., J.Y., M.C. (Mike Collyer); review/editing, all authors; methodology, all authors; supervision, C.L.K.R. and M.C. (Maycira Costa); writing—original draft preparation, N.R.H.; formal analysis, N.R.H.; funding acquisition, J.Y., J.S. and C.L.K.R.; software, M.C. (Mike Collyer); resources, J.S., J.Y., C.L.K.R.; visualization, N.R.H.; project administration, J.S., J.Y., M.C. (Maycira Costa)., C.L.K.R. All authors have read and agreed to the published version of the manuscript.

Funding: This research was funded by Comox Valley Project Watershed Society (BC Salmon Restoration and Innovation Fund), Parks Canada (Southern Resident Killer Whale research project), and the Costa NSERC Discover Grant.

Data Availability Statement: Data can be accessed here: https://github.com/nicolahoutman/Drone-Map-Fish. Created 13 October 2022.

Acknowledgments: Field work was not possible without the resources, logistical planning, and personnel provided by Pacific Rim National Park Reserve through the Southern Resident Killer Whale research project. We thank Krista Bohlen and Rick Ward for providing field work assistance and Alejandra Mora-Soto and Vishnu Perumthuruthil Suseelan for providing statistical analysis assistance.

Conflicts of Interest: The authors declare no conflict of interest. The funders had no role in the design of the study; in the collection, analyses, or interpretation of data; in the writing of the manuscript; or in the decision to publish the results.

References

1. Harris, J.M.; Nelson, J.; Rieucau, G.; Broussard III, W.P. Use of drones in fishery science. *Trans. Am. Fish. Soc.* **2019**, *148*, 687–697. [CrossRef]
2. Arimitsu, M.L.; Piatt, J.F.; Heflin, B.; Biela, V.; Schoen, S.K. Monitoring long-term changes in forage fish distribution, abundance and body condition. *Exxon Valdez* Oil Spill Restoration Project Final Report (Restoration Project 16120114-O). In *Exxon Valdez*; Oil Spill Trustee Council: Anchorage, Alaska, 2018.
3. Schofield, G.; Esteban, N.; Katselidis, K.A.; Hays, G.C. Drones for research on sea turtles and other marine vertebrates—A review. *Biol. Conserv.* **2019**, *238*, 108214. [CrossRef]
4. Joyce, K.E.; Duce, S.; Leahy, S.M.; Leon, J.; Maier, S.W. Principles and practice of acquiring drone-based image data in marine environments. *Mar. Freshw. Res.* **2019**, *70*, 952–963. [CrossRef]
5. Raoult, V.; Colefax, A.P.; Allan, B.M.; Cagnazzi, D.; Castelblanco-Martínez, N.; Ierodiaconou, D.; Johnston, D.W.; Landeo-Yauri, S.; Lyons, M.; Pirotta, V.; et al. Operational protocols for the use of drones in marine animal research. *Drones* **2020**, *4*, 64. [CrossRef]
6. Pikitch, E.K.; Rountos, K.J.; Essington, T.E.; Santora, C.; Pauly, D.; Watson, R.; Sumaila, U.R.; Boersma, P.D.; Boyd, I.L.; Conover, D.O.; et al. The global contribution of forage fish to marine fisheries and ecosystems. *Fish Fish.* **2014**, *15*, 43–64. [CrossRef]
7. Pikitch, E.; Boersma, P.D.; Boyd, I.; Conover, D.; Cury, P.; Essington, T.; Heppell, S.; Houde, E.; Mangel, M.; Pauly, D.; et al. *Little Fish, Big Impact: Managing a Crucial Link in Ocean Food Webs. Lenfest Forage Fish Task Force*; Lenfest Ocean Program: Washington, DC, USA, 2012; pp. 1–120.
8. Gaydos, J.K.; Pearson, S.F. Birds and mammals that depend on the Salish Sea: A compilation. *Northwestern Nat.* **2011**, *92*, 79–94. [CrossRef]
9. Duguid, W.D.; Boldt, J.L.; Chalifour, L.; Greene, C.M.; Galbraith, M.; Hay, D.; Lowry, D.; McKinnell, S.; Neville, C.M.; Qualley, J.; et al. Historical fluctuations and recent observations of Northern Anchovy Engraulis mordax in the Salish Sea. *Deep. Sea Res. Part II Top. Stud. Oceanogr.* **2019**, *159*, 22–41. [CrossRef]
10. Osgood, G.J.; Kennedy, L.A.; Holden, J.J.; Hertz, E.; McKinnell, S.; Juanes, F. Historical diets of forage fish and juvenile pacific salmon in the strait of Georgia, 1966–1968. *Mar. Coast. Fish.* **2016**, *8*, 580–594. [CrossRef]
11. Therriault, T.W.; Hay, D.E.; Schweigert, J.F. Biologic overview and trends in pelagic forage fish abundance in the Salish Sea (Strait of Georgia, British Columbia). *Mar. Ornithol.* **2009**, *37*, 3–8.
12. Beamish, R.J.; Lange, K.L.; Neville, C.M.; Sweeting, R.M.; Beacham, T.D. Structural patterns in the distribution of ocean-and stream-type juvenile Chinook Salmon populations in the Strait of Georgia in 2010 during the critical early marine period. *NPAFC Doc.* **2011**, *1354*, 27.
13. 2020, p. 203. Available online: https://www.canada.ca/en/environmentclimate-change/services/species-risk-public-registry.html (accessed on 23 July 2020).
14. 2012, p. 82. Available online: www.registrelep-sararegistry.gc.ca/default_e.cfm (accessed on 23 July 2020).
15. Therriault, T.W.; McDiarmid, A.N.; Wulff, W.; Hay, D.E. Review of surf smelt (Hypomesus pretiosus) biology and fisheries, with suggested management options for British Columbia. *DFO Can. Sci. Advis. Sec. Res. Doc.* **2002**, *115*, 1–37.
16. Therriault, T.W.; McDiarmid, A.N.; Wulff, W.; Hay, D.E. A review of northern anchovy (Engraulis mordax) biology and fisheries with suggested management options for British Columbia. *DFO Can. Sci. Advis. Sec. Res. Doc.* **2002**, *112*, 1–27.
17. Fisheries and Oceans Canada. Wild Salmon Policy, Annual Report 2019–2020. Available online: https://waves-vagues.dfo-mpo.gc.ca/library-bibliotheque/41031970.pdf (accessed on 5 June 2020).
18. Boldt, J.L.; Murphy, H.; Chamberland, J.-M.; Debertin, A.J.; Gauthier, S.; Hackett, B.; Hagel, P.S.; Majewski, A.R.; McDermid, J.L.; Merette, D.; et al. Canada's forage fish: An important but poorly understood component of marine ecosystems. *Can. J. Fish. Aquat. Sci.* **2022**, *79*, 1911–1933. [CrossRef]
19. Cleguer, C.; Kelly, N.; Tyne, J.; Wieser, M.; Peel, D.; Hodgson, A. A novel method for using small unoccupied aerial vehicles to survey wildlife species and model their density distribution. *Front. Mar. Sci.* **2021**, *8*, 462. [CrossRef]

20. Shaffer, S. Preferential use of nearshore kelp habitats by juvenile salmon and forage fish. In Proceedings of the 2003 Georgia Basin/Puget Sound Research Conference, Vancouver, BC, Canada, 31 March 2003; Available online: https://www.researchgate.net/profile/Anne-Shaffer/publication/242213830_Preferential_use_of_Nearshore_Kelp_Habitats_by_Juvenile_Salmon_and_Forage_Fish/links/5567aa5f08aec2268300ffb5/Preferential-use-of-Nearshore-Kelp-Habitats-by-Juvenile-Salmon-and-Forage-Fish.pdf (accessed on 4 August 2020).
21. Doukari, M.; Batsaris, M.; Papakonstantinou, A.; Topouzelis, K. A protocol for aerial survey in coastal areas using UAS. *Remote Sens.* **2019**, *11*, 1913. [CrossRef]
22. Nahirnick, N.K.; Reshitnyk, L.; Campbell, M.; Hessing-Lewis, M.; Costa, M.; Yakimishyn, J.; Lee, L. Mapping with confidence; delineating seagrass habitats using Unoccupied Aerial Systems (UAS). *Remote Sens. Ecol. Conserv.* **2019**, *5*, 121–135. [CrossRef]
23. Colefax, A.P.; Butcher, P.A.; Pagendam, D.E.; Kelaher, B.P. Reliability of marine faunal detections in drone-based monitoring. *Ocean. Coast. Manag.* **2019**, *174*, 108–115. [CrossRef]
24. Colefax, A.P.; Butcher, P.A.; Kelaher, B.P. The potential for unmanned aerial vehicles (UAVs) to conduct marine fauna surveys in place of manned aircraft. *ICES J. Mar. Sci.* **2018**, *75*, 1–8. [CrossRef]
25. Marsh, H.; Sinclair, D.F. Correcting for visibility bias in strip transect aerial surveys of aquatic fauna. *J. Wildl. Manag.* **1989**, *53*, 1017–1024. [CrossRef]
26. Brack, I.V.; Kindel, A.; Oliveira, L.F.B. Detection errors in wildlife abundance estimates from Unmanned Aerial Systems (UAS) surveys: Synthesis, solutions, and challenges. *Methods Ecol. Evol.* **2018**, *9*, 1864–1873. [CrossRef]
27. Barnas, A.F.; Chabot, D.; Hodgson, A.J.; Johnston, D.W.; Bird, D.M.; Ellis-Felege, S.N. A standardized protocol for reporting methods when using drones for wildlife research. *J. Unmanned Veh. Syst.* **2020**, *8*, 89–98. [CrossRef]
28. Nahirnick, N.K.; Hunter, P.; Costa, M.; Schroeder, S.; Sharma, T. Benefits and challenges of UAS imagery for eelgrass (Zostera marina) mapping in small estuaries of the Canadian west coast. *J. Coast. Res.* **2019**, *35*, 673–683. [CrossRef]
29. Colefax, A.P.; Kelaher, B.P.; Walsh, A.J.; Purcell, C.R.; Pagendam, D.E.; Cagnazzi, D.; Butcher, P.A. Identifying optimal wavelengths to maximise the detection rates of marine fauna from aerial surveys. *Biol. Conserv.* **2021**, *257*, 109102. [CrossRef]
30. Doukari, M.; Topouzelis, K. Overcoming the UAS limitations in the coastal environment for accurate habitat mapping. *Remote Sens. Appl. Soc. Environ.* **2022**, *26*, 100726. [CrossRef]
31. Doukari, M.; Batsaris, M.; Topouzelis, K. UASea: A data acquisition toolbox for improving marine habitat mapping. *Drones* **2021**, *5*, 73. [CrossRef]
32. U.S. NOAA Coastal Services Center. Guidance for Benthic Habitat Mapping: An Aerial Photographic Approach by Mark Finkbeiner [and by] Bill Stevenson and Renee Seaman, Technology Planning and Management Corporation, Charleston, SC. (NOAA/CSC/20117-PUB). 2001. Available online: http://hdl.handle.net/1834/20029 (accessed on 5 June 2020).
33. Mount, R. Acquisition of through-water aerial survey images. *Photogramm. Eng. Remote Sens.* **2005**, *71*, 1407–1415. [CrossRef]
34. Haynes, T.B. Modeling Habitat Use of Young-of-the-Year Pacific Sand Lance (Ammodytes Hexapterus) in the Nearshore Region of Barkley Sound, British Columbia. Master's Thesis, University of Victoria, Victoria, BC, Canada, 2006.
35. Robinson, C.L.; Yakimishyn, J. The persistence and stability of fish assemblages within eelgrass meadows (*Zostera marina*) on the Pacific coast of Canada. *Can. J. Fish. Aquat. Sci.* **2013**, *70*, 775–784. [CrossRef]
36. Robinson, C.L.; Proudfoot, B.; Rooper, C.N.; Bertram, D.F. Comparison of spatial distribution models to predict subtidal burying habitat of the forage fish ammodytes personatus in the Strait of Georgia, British Columbia, Canada. *Aquat. Conserv. Mar. Freshw. Ecosyst.* **2021**, *31*, 2855–2869. [CrossRef]
37. Moore, R.D.; Spittlehouse, D.L.; Whitfield, P.H.; Stahl, K. Weather and climate. In *Compendium of Forest Hydrology And Geomorphology in British Columbia*, 1st ed.; Province of British Columbia: Victoria, BC, Canada, 2010; Volume 1, pp. 47–84.
38. Bourdon, R. Interactions between fish communities and shellfish aquaculture in Baynes Sound, British Columbia. Master's Thesis, University of Victoria, Victoria, BC, Canada, 2015.
39. Levings, C. Overview of baynes sound salmonids and possible limiting factors important for local ecosystem management. In *Stewarding the Sound*, 1st ed.; CRC Press: Boca Raton, FL, USA, 2019; Volume 1, pp. 41–50.
40. Bendell, L.I. Favored use of anti-predator netting (APN) applied for the farming of clams leads to little benefits to industry while increasing nearshore impacts and plastics pollution. *Mar. Pollut. Bull.* **2015**, *91*, 22–28. [CrossRef]
41. Sakurai, Y.; Quéro, J.C. Schooling finfish (cods, herrings, sardines, mackerels, and others). In *Encylopedia of Life Support Systems: Fisheries and Aquaculture*, 1st ed.; Sadan, P., Ed.; Eolss Publishers Co. Ltd.: Oxford, UK, 2009.
42. Cott, H.B. Obliterate shading. In *Adaptive Coloration in Animals*, 2nd ed.; Methuen & Co.: London, UK, 1940; Volume 1, pp. 35–46.
43. Butcher, P.A.; Colefax, A.P.; Gorkin, R.A.; Kajiura, S.M.; López, N.A.; Mourier, J.; Purcell, C.R.; Skomal, G.B.; Tucker, J.P.; Walsh, A.J.; et al. The drone revolution of shark science: A review. *Drones* **2021**, *5*, 8. [CrossRef]
44. Verschuur, G.L. Transparency measurements in Garner Lake, Tennessee: The relationship between Secchi depth and solar altitude and a suggestion for normalization of Secchi depth data. *Lake Reserv. Manag.* **1997**, *13*, 142–153. [CrossRef]
45. NOAA Sun Calculator. Available online: https://www.esrl.noaa.gov/gmd/grad/solcalc/ (accessed on 20 June 2020).
46. Beaufort Wind Scale Table. Available online: https://www.canada.ca/en/environment-climate-change/services/general-marine-weather-information/understanding-forecasts/beaufort-wind-scale-table.html (accessed on 20 June 2020).
47. Paliy, O.; Shankar, V. Application of multivariate statistical techniques in microbial ecology. *Mol. Ecol.* **2016**, *25*, 1032–1057. [CrossRef] [PubMed]

48. Chok, N.S. Pearson's versus Spearman's and Kendall's Correlation Coefficients for Continuous Data. Master's Thesis, University of Pittsburgh, Pittsburgh, PE, USA, 2010.
49. R Core Team. R: A Language and Environment For Statistical Computing. R Foundation for Statistical Computing, Vienna, Austria. Available online: http://www.R-project.org/ (accessed on 14 November 2021).
50. Hartigan, J.A.; Wong, M.A. Algorithm AS 136: A K-means clustering algorithm. *Appl. Stat.* **1979**, *28*, 100–108. [CrossRef]
51. Dray, S.; Dufour, A. The ade4 package: Implementing the duality diagram for ecologists. *J. Stat. Softw.* **2007**, *22*, 1–20. [CrossRef]
52. Wei, T.; Simko, V. R Package 'Corrplot': Visualization of a Correlation Matrix (Version 0.92). Available online: https://github.com/taiyun/corrplot (accessed on 20 February 2022).
53. Nahirnick, N.K. Long-Term Spatial-Temporal Eelgrass (Zostera Marina) Habitat Change (1932–2016) in the Salish Sea Using Historic Aerial Photography and Unmanned Aerial Vehicle. Master's Thesis, University of Victoria, Victoria, BC, Canada, 2018.
54. Liu, W.C. Water column light attenuation estimation to simulate phytoplankton population in tidal estuary. *Environ. Geol.* **2005**, *49*, 280–292. [CrossRef]
55. Kirk, J.T. *Light and Photosynthesis in Aquatic Ecosystems*, 1st ed.; Cambridge University Press: Cambridge, UK, 1994.
56. Lee, Z.; Shang, S.; Hu, C.; Du, K.; Weidemann, A.; Hou, W.; Junfang, L.; Lin, G. Secchi disk depth: A new theory and mechanistic model for underwater visibility. *Remote Sens. Environ.* **2015**, *169*, 139–149. [CrossRef]
57. Chabot, D.; Bird, D.M. Evaluation of an off-the-shelf unmanned aircraft system for surveying flocks of geese. *Waterbirds* **2012**, *35*, 170–174. [CrossRef]
58. Patterson, C.; Koski, W.; Pace, P.; McLuckie, B.; Bird, D.M. Evaluation of an unmanned aircraft system for detecting surrogate caribou targets in Labrador. *J. Unmanned Veh. Syst.* **2015**, *4*, 53–69. [CrossRef]
59. Pollock, K.H.; Marsh, H.D.; Lawler, I.R.; Alldredge, M.W. Estimating animal abundance in heterogeneous environments: An application to aerial surveys for dugongs. *J. Wildl. Manag.* **2006**, *70*, 255–262. [CrossRef]
60. Fuentes, M.M.P.B.; Bell, I.; Hagihara, R.; Hamann, M.; Hazel, J.; Huth, A.; Seminoff, J.A.; Marsh, H. Improving in-water estimates of marine turtle abundance by adjusting aerial survey counts for perception and availability biases. *J. Exp. Mar. Biol. Ecol.* **2015**, *471*, 77–83. [CrossRef]
61. Haynes, T.B.; Robinson, C.L. Re-use of shallow sediment patches by Pacific sand lance (*Ammodytes hexapterus*) in Barkley Sound, British Columbia, Canada. *Environ. Biol. Fishes* **2011**, *92*, 1–12. [CrossRef]
62. Hagihara, R.; Jones, R.E.; Sobtzick, S.; Cleguer, C.; Garrigue, C.; Marsh, H. Compensating for geographic variation in detection probability with water depth improves abundance estimates of coastal marine megafauna. *PLoS ONE* **2018**, *13*, 1–15. [CrossRef] [PubMed]